Bending and pinching of three-phase stripes: From secondary instabilities to morphological deformations in organic photovoltaics

Alon Z. Shapira,[1] Nir Gavish,[2] Hannes Uecker,[3] and Arik Yochelis[4,5,*]

[1]*Swiss Institute for Dryland Environmental and Energy Research, Blaustein Institutes for Desert Research, Ben-Gurion University of the Negev, Sede Boqer Campus, Midreshet Ben-Gurion 8499000, Israel*

[2]*Department of Mathematics, Technion - IIT, Haifa 3200003, Israel*

[3]*Institute for Mathematics, Carl von Ossietzky University of Oldenburg, P.F 2503, 26111 Oldenburg, Germany*

[4]*Department of Solar Energy and Environmental Physics, Blaustein Institutes for Desert Research, Ben-Gurion University of the Negev, Sede Boqer Campus, Midreshet Ben-Gurion 8499000, Israel*

[5]*Department of Physics, Ben-Gurion University of the Negev, Beer Sheva 8410501, Israel*

(Received 30 September 2020; accepted 16 November 2020; published 15 December 2020)

Optimizing the properties of the mosaic nanoscale morphology of bulk heterojunction (BHJ) organic photovoltaics (OPV) is not only challenging technologically but also intriguing from the mechanistic point of view. Among the recent breakthroughs is the identification and utilization of a three-phase (donor-mixed-acceptor) BHJ, where the (intermediate) mixed phase can inhibit mesoscale morphological changes, such as phase separation. Using a mean-field approach, we reveal and distinguish between generic mechanisms that alter, through transverse instabilities, the evolution of stripes: the bending (zigzag mode) and the pinching (cross-roll mode) of the donor-acceptor domains. The results are summarized in a parameter plane spanned by the mixing energy and illumination, and show that donor-acceptor mixtures with higher mixing energy are more likely to develop pinching under charge-flux boundary conditions. The latter is notorious as it leads to the formation of disconnected domains and hence to loss of charge flux. We believe that these results provide a qualitative road map for BHJ optimization, using mixed-phase composition and, therefore, an essential step toward long-lasting OPV. More broadly, the results are also of relevance to study the coexistence of multiple-phase domains in material science, such as in ion-intercalated rechargeable batteries.

DOI: 10.1103/PhysRevE.102.062213

I. INTRODUCTION

Organic photovoltaics (OPV) have been subjected to intensive research over the past two decades, not only due to their potential advantages as portable and/or lightweight technological devices but also for their intriguing physicochemical mechanisms of operation [1–4]. At the heart of the OPV is the nanoscale mosaic active layer of electron donor (D) and electron acceptor (A) materials, i.e., the so-called bulk heterojunction (BHJ) [5–11]. This subtle morphology is essential for the efficient dissociation of excitons at the D-A interfaces to electrons and holes and for transport of the latter toward the collectors [12–14]. The short lifetime of the excitons is translated to a spatial length scale, also known as the *diffusion length*, which, respectively, sets about tens of nanometer bicontinuous (ideally, comblike) morphology [11,15–24].

Recent evidence, however, indicates that in some compositions [4,25–33], a third phase, which is being referred to as a *mixed phase* (MP), may additionally become stable along with the pure D-A phases [34,35]. This MP has a molecular percolating structure about a 1:1 ratio between the donor and the acceptor molecules [35] and thus is distinct from a random distribution, although in both cases the averaged quantity is similar. As such, the MP can be thought of as a distinct energetic barrier (as being an intermediate metastable state) between the energetically favorable D and A phases [35,36], while keeping the exciton dissociation properties intact. Recent studies indicate that MP plays a role in the evolution of BHJ, ranging from the width and form of the D-A interface [25,36,37] to an inhibitor of the phase separation process [35].

Motivated by three-phase OPV experiments, we study how the intermediate mixed phase may affect the transverse instabilities of striped BHJ by distinguishing between two generic modes and the respective role of the boundary conditions (BC): the bending (zigzag) mode and the pinching (cross-roll) mode that is critical for operation since it destroys the flux of charges to collectors, as schematically demonstrated in Fig. 1. We use a recently proposed Shapira-Gavish-Yochelis mean-field model [36] that incorporates the morphological evolution of a three-phase BHJ under illumination and, for analysis, we employ the generalized eigenvalue methodology [38,39] to identify the instability onsets. Specifically, we elaborate on how the stability of the BHJ to pinching depends on the increase of the energetic barrier of the mixing energy, i.e., the depth of the intermediate well in the free energy, and exemplify the results in the parameter plane spanned by well depth and illumination strength. The generic nature of the results provides a plausible strategy to control the morphological stability of the BHJ under illumination.

*yochelis@bgu.ac.il

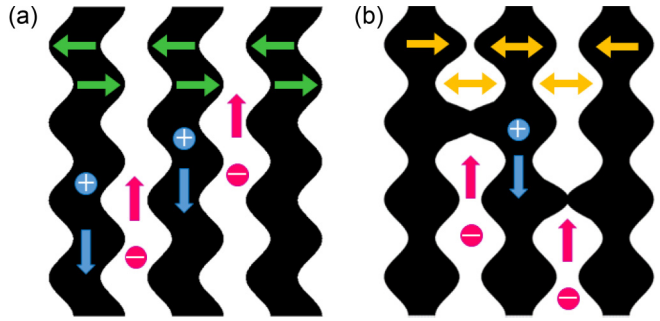

FIG. 1. Illustrations of (a) the bending zigzag (ZZ) and (b) the cross-roll (CR) instabilities. Horizontal arrows indicate the bending direction, while vertical arrows show the directions of the opposite charge fluxes to the electrodes.

II. DETERMINING THE DONOR-ACCEPTOR RATIO

In the dark, the free energy comprises the entropy and the mixing energy for the material order parameter [36], $u := \varphi_A - \varphi_D \in [-1, 1]$, where φ_A, φ_D are the respective fractions of the A-D phases. Its dimensionless form reads

$$\mathcal{E}_M(u) = \int_\Omega \underbrace{\frac{1-u}{2}\ln\frac{1-u}{2}}_{\text{donor's entropy}} + \underbrace{\frac{1+u}{2}\ln\frac{1+u}{2}}_{\text{acceptor's entropy}} + \underbrace{\frac{\beta}{2}(1-u^2)(u^2+\xi) + \frac{\lambda}{2}|\nabla u|^2 - e_0}_{\text{mixing energy}}\, dx, \quad (1)$$

where Ω is the domain, which we take to be a rectangle, $\Omega = (0, l_x) \times (0, l_y)$. Further, e_0 is a reference energy density for which the minimum of $\mathcal{E}_M$ is zero, β determines the ratio between mixing energy and entropy, and ξ determines the depth of the intermediate well such that small ξ corresponds to a lower mixing energy [see Fig. 2(a)], and λ is the penalty for the creation of multiple interfaces and associated with the width of the interface. Due to entropy, the minimum energies of donor-rich ($u := u_-$) and acceptor-rich ($u := u_+$) phases are shifted from $u = \pm 1$ to slightly lower values in $|u|$, while the mixed phase always sits at $u := u_0 = 0$, as shown in Fig. 2(a). Due to conservation of the order parameter, however, there are many other uniform solutions $u = u_*$ and these solutions are related to the D:A ratio of nonuniform solutions, e.g., D-A interfaces. The connection between the u_* and the D:A ratio is made through averaging of u in one space dimension (1D),

$$\langle u\rangle := l_x^{-1}\int_0^{l_x} u\,dx. \quad (2)$$

For the *symmetric* case $\langle u\rangle = 0$, the amount of donor and acceptor is identical so that the interface is located at $x = l_x/2$, and for the *asymmetric* case, where $|\langle u\rangle| > 0$, this location is shifted; note that for the uniform states, $\langle u\rangle = u_*$. Thus, for the nonuniform solutions that are of interest here, it is required to identify the allowed range of $\langle u\rangle$ and we do it by looking at the stability of u_*.

The evolution equation [36] [in the dark and with mobility $D_u(1-u^2)$] reads

$$\frac{\partial u}{\partial t} = D_u\frac{\partial^2 u}{\partial x^2} + D_u\frac{\partial}{\partial x}\left\{(1-u^2)\left[\beta(1-6u^2-\xi)\frac{\partial u}{\partial x} - \lambda\frac{\partial^3 u}{\partial x^3}\right]\right\}, \quad (3)$$

where D_u is the diffusion coefficient. Linear stability analysis (performed on an infinite domain) about uniform states $u = u_*$ corresponds to

$$u - u_* \propto e^{\alpha t + ikx} + \text{c.c.}, \quad (4)$$

where c.c. is the complex conjugate and α is the perturbation growth rate of wave number k and is given by

$$\alpha(k) = -D_u k^2\{1 + (1-u_*^2)[\beta(1-6u_*^2-\xi) + \lambda k^2]\}. \quad (5)$$

The instability of $u = u_*$ is of a typical long-wave-number type [40] and the regime of unstable steady state solutions, $u_*^{\min} < |u_*| < u_*^{\max}$, is obtained by taking the limit $\alpha(k) \to 0$

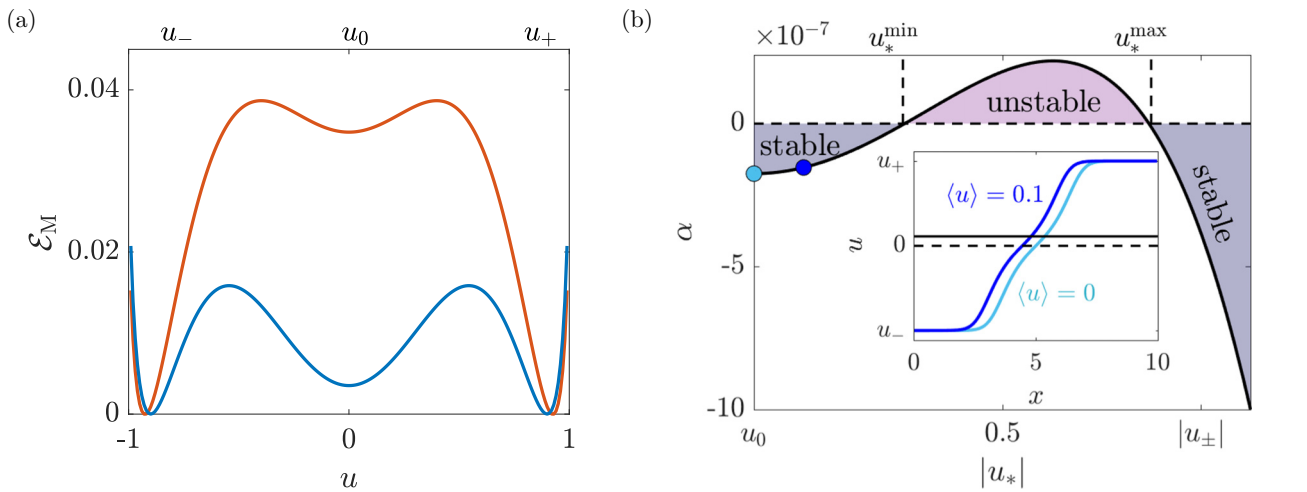

FIG. 2. (a) Free energy functional (1) for uniform u, with $\xi = 2.65$, $e_0 = -0.034$ (blue, genuine triple well) and $\xi = 2.8$, $e_0 = 0.028$ (red, closer to double well), where ξ corresponds to the mixing energy. (b) Stability and instability intervals for uniform solutions determined by the critical values $u_*^{\min} \approx 0.30$ and $u_*^{\max} \approx 0.80$. The inset demonstrates three-phase interface solutions, as computed from (3), for $\langle u\rangle = 0$ and $\langle u\rangle = 0.1$ (as marked by • in the main figure, respectively); the location of the interface with $\langle u\rangle = 0$ is at $x = 0$. The horizontal solid and dashed lines indicate the value $u_* = \langle u\rangle = 0.1$ and $u_* = \langle u\rangle = 0$, respectively. Parameters: $D_u = 1$, $\beta = 0.5$, $\xi = 2.65$, $\lambda = 0.1$, $k = 10^{-3}$, $l_x = 10$.

as $k \to 0$ [see Fig. 2(b)], where

$$u_*^{\min} = \frac{1}{2\sqrt{3}}\sqrt{7-\xi-\sqrt{(5+\xi)^2-24/\beta}},$$
$$u_*^{\max} = \frac{1}{2\sqrt{3}}\sqrt{7-\xi+\sqrt{(5+\xi)^2-24/\beta}}.$$

These results imply that any choice within the $u_*^{\min} < |u_*| < u_*^{\max}$ range will result in a coarsening dynamics that minimizes the energetic penalty of the interfaces, following which phase separation is achieved (not shown here). In the inset of Fig. 2(b), we show that indeed the interface solutions are bi-asymptotic to $u_\pm$ and that the location of the interface shifts according to $\langle u\rangle$ that is set by u_*. Thus, in the analysis that follows, we will focus on the regime $0 < |u_*| < u_*^{\min}$, under illumination.

III. EXISTENCE OF STRIPES UNDER ILLUMINATION AND THE EFFECT OF D-A ASYMMETRY

Illumination leads to the creation of excitons which dissociate at the D-A interface and thus drive the BHJ out of equilibrium. The (dimensionless) total free energy under illumination takes the form [36]

$$\mathcal{E} = \mathcal{E}_{\rm M} + \int_\Omega \underbrace{\chi\ln\chi + p\ln p + n\ln n}_{\text{charges entropy}} + \underbrace{\phi(p-n) - \frac{\epsilon}{2}|\nabla\phi|^2}_{\text{electrostatic energy}} + \underbrace{\frac{\zeta}{2}[p(1+u)^2 + n(1-u)^2]}_{\text{charge affinity}}\,dx,$$

where the corresponding equations of motion also incorporate the generation and recombination following Buxton and Clarke [41], and fluxes of electrical charges coupled to morphological evolution of the BHJ order parameter [36]:

$$\frac{\partial u}{\partial t} = \underbrace{D_u\nabla^2 u + D_u\nabla\cdot\{(1-u^2)[\beta(1-6u^2-\xi)\nabla u - \lambda\nabla^3 u]\}}_{\text{phase separation}} + \underbrace{D_u\zeta\nabla\cdot\{(1-u^2)[(p+n)\nabla u + (1+u)\nabla p - (1-u)\nabla n]\}}_{\text{donor/acceptor affinity to charges}}, \tag{6a}$$

$$\frac{\partial\chi}{\partial t} = \underbrace{\nabla^2\chi}_{\text{diffusion}} - \underbrace{\tau^{-1}(1-u^2)\chi}_{\text{dissociation}} - \underbrace{\chi}_{\text{decay}} + \underbrace{G}_{\text{generation}}, \tag{6b}$$

$$\frac{\partial p}{\partial t} = D_p\nabla\cdot[\underbrace{p\nabla\phi + \nabla p}_{\text{drift-diffusion}} + \underbrace{\zeta p(1+u)\nabla u}_{\text{charge affinity}}] + \tau^{-1}(1-u^2)\chi - \underbrace{\gamma np}_{\text{recombination}}, \tag{6c}$$

$$\frac{\partial n}{\partial t} = D_n\nabla\cdot[-n\nabla\phi + \nabla n - \zeta n(1-u)\nabla u] + \tau^{-1}(1-u^2)\chi - \gamma np, \tag{6d}$$

$$0 = \nabla\cdot[\epsilon\nabla\phi] + p - n. \tag{6e}$$

Here the fields χ, p, n stand for excitons, holes, and electrons, respectively, ϕ is the electric potential, D_p, D_n are the respective diffusion constants, ζ is the interaction energy between the electrical charges and donor-acceptor compositions, τ is the exciton's dissociation time, G is the exciton's generation rate, γ is the electron-hole recombination rate, and ϵ is the permittivity. For details we refer the reader to Shapira *et al.* [36].

Uniform solutions of system (6) are given by

$$\mathbf{U}_* = (u_*, \chi_*, p_*, n_*, 0)^T,$$

where

$$\chi_* = \tau G/(\tau + 1 - u_*^2),$$
$$p_* = n_* = \sqrt{G(1-u_*^2)/[\gamma(\tau+1-u_*^2)]},$$

and T stands for transpose. Linear analysis in 1D, by replacing $u(x)$ with $\mathbf{U}(x)$, shows that in the range $0 \leqslant |u_*| < u_*^{\min}$, the uniform solution $\mathbf{U}_*$ goes through a subcritical finite wavenumber instability at $G = G_c$, giving rise to periodic solutions $\mathbf{U}_\ell(x)$ with wave number k_c, that corresponds to the spatial wavelength $\ell_c = 2\pi/k_c$, where for $u_* = 0$ we get

$$G_c = \frac{\epsilon^2\gamma(\tau+1)(\beta\xi-\beta-1)^2}{4(\lambda-\epsilon\zeta+\epsilon\zeta^2-2\zeta\sqrt{\epsilon\lambda})^2}$$

and

$$k_c^2 = \frac{(1-\zeta\sqrt{\epsilon/\lambda})(\beta\xi-\beta-1)}{\lambda-\epsilon\zeta+\epsilon\zeta^2-2\zeta\sqrt{\epsilon\lambda}},$$

while for $|u_*| > 0$ the critical values are computed numerically. The periodic solutions

$$\mathbf{U}_\ell(x) = [u_\ell(x), \chi_\ell(x), p_\ell(x), n_\ell(x), \phi_\ell(x)]^T$$

bifurcate toward the stable portion of $\mathbf{U}_*$, which is in the direction $G < G_c$, and thus are initially unstable. Then they grow in amplitude and stabilize after the saddle node bifurcation that is located close to $G = 0$, and continue to be stable as G increases, as shown in Fig. 3(a).

Notably, conservation of the order parameter u also forces the periodic solutions u_ℓ to keep the average value that is initially set by u_*. Namely, periodic solutions (which can be extended in the y direction to form stripes) that bifurcate from $u_* = 0$ correspond to *symmetric* stripes (i.e., identical width of the donor and the acceptor domains), while periodic solutions that bifurcate from $u_* = 0.1$, for example, are *asymmetric*, in which acceptor domains are wider; the latter is demonstrated in Fig. 3(b). Next, we

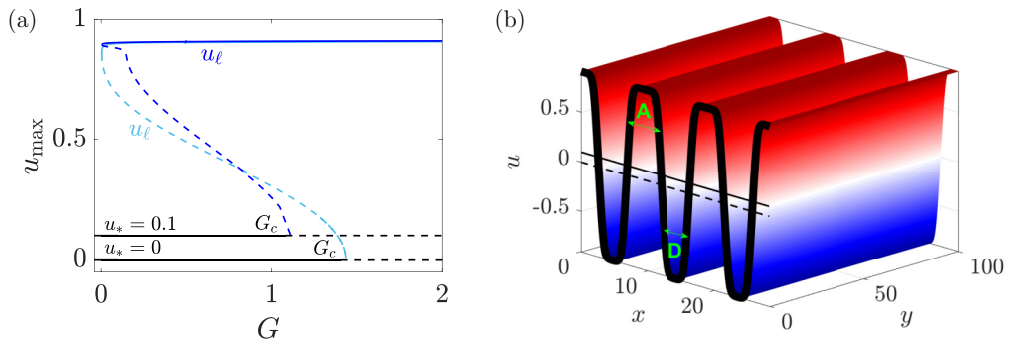

FIG. 3. (a) Bifurcation diagram showing the branches of symmetric (cyan) and asymmetric (blue) periodic solutions in 1D, u_ℓ, computed for system (6); solid (dashed) lines indicate stable (unstable) solutions. For these computations, we employed the numerical continuation package PDE2PATH [42,43], with periodic BC. The periodic solutions bifurcate from the uniform solutions $u_* = 0$ and $u_* = 0.1$ at the respective values of $G = G_c$. (b) Asymmetric stripe pattern plotted at $G = 2$ after extending u_ℓ in the y direction. The solid horizontal line indicates $\langle u \rangle = 0.1$. The arrows at $u = \pm 0.5$ indicate the width of the acceptor (A) and donor (D) phases, with A being wider. The domain size is $\Omega = [0, 3\ell_c] \times [0, 100]$ and the critical wavelength of u_ℓ is $\ell_c \approx 9.38$. Parameters: $\beta = 0.5, \xi = 2.65, \lambda = 0.1, \zeta = 4, \epsilon = 0.25, \tau = \gamma = 100$, $D_p = D_n = 3, D_u = 1$.

calculate the stability properties of stripes in the transverse direction.

IV. TRANSVERSE INSTABILITY OF THREE-PHASE DONOR-MIXED-ACCEPTOR STRIPES

For the linear transverse instability analysis of stripes to zigzag (ZZ) that corresponds to bending and to cross roll (CR) that causes pinching (see Fig. 1), we employ a general space-dependent eigenvalue method [44–50] that has been used, for example, in the context of convection rolls, stripes in reaction-diffusion media, and thin fluid films. However, due to application to OPV, our interest here is to reveal the impact of physical boundary conditions on the instability of stripes, i.e., on nonperiodic domains in y directions.

A. Linear analysis on unbounded domains

We start by performing a general analysis of stripes on nonphysical infinite (periodic in the y direction) domains [39],

$$\mathbf{U}(t, x, y) - \mathbf{U}_\ell(x) \propto \tilde{\mathbf{U}}(x) e^{\eta t + i k_y y} + \text{c.c.}, \tag{7}$$

where η is the growth rate of the wave number, k_y, in the transverse direction to $\mathbf{U}_\ell(x)$, and

$$\tilde{\mathbf{U}}(x) = [\tilde{u}(x), \tilde{\chi}(x), \tilde{p}(x), \tilde{n}(x), \tilde{\phi}(x)]^T$$

is always the periodic eigenfunction. This formulation introduces a generalized eigenvalue system,

$$\eta \mathcal{M} \tilde{\mathbf{U}} = \mathcal{L} \tilde{\mathbf{U}}. \tag{8}$$

In (8), $\mathcal{M}$ is a singular projection matrix [38],

$$\mathcal{M} = \begin{pmatrix} 1 & 0 & 0 & 0 & 0 \\ 0 & 1 & 0 & 0 & 0 \\ 0 & 0 & 1 & 0 & 0 \\ 0 & 0 & 0 & 1 & 0 \\ 0 & 0 & 0 & 0 & 0 \end{pmatrix}, \tag{9}$$

and $\mathcal{L}$ is a linear operator,

$$\mathcal{L}[\mathbf{U}_\ell; k_y] = \begin{pmatrix} D_u \mathcal{L}_{1,1} & 0 & D_u \mathcal{L}_{1,3} & D_u \mathcal{L}_{1,4} & 0 \\ 2\chi u/\tau & \mathcal{L}_{2,2} & 0 & 0 & 0 \\ \mathcal{L}_{3,1} & (1-u^2)/\tau & \mathcal{L}_{3,3} & -\gamma p & \mathcal{L}_{3,5} \\ \mathcal{L}_{4,1} & (1-u^2)/\tau & -\gamma n & \mathcal{L}_{4,4} & \mathcal{L}_{4,5} \\ 0 & 0 & 1 & -1 & \epsilon\left(\hat{\partial}_x^2 - k_y^2\right) \end{pmatrix}, \tag{10}$$

where $\mathcal{L}_{1,1} = \lambda[1-u^2]\partial_x^4 + 2\lambda u u_x \partial_x^3 + \mathcal{L}_{1,1}^{(0)} + \mathcal{L}_{1,1}^{(1)}\partial_x + \mathcal{L}_{1,1}^{(2)}\partial_x^2$,

$$\begin{aligned}
\mathcal{L}_{1,1}^{(0)} &= \big(\lambda\big[2uu_{xxxx} + 2u_x u_{xxx} - k_y^4(1-u^2)\big] + \beta\big\{u_{xx}(24u^3 - 14u) + u_x^2(72u^2 - 14) - k_y^2(6u^4 - 7u^2 + 1) \\
&\quad + \xi\big[2u_x^2 + 2uu_{xx} + k_y^2(1-u^2)\big]\big\} + \zeta\big\{p_{xx}(1 - 2u - 3u^2) + n_{xx}(1 + 2u - 3u^2) \\
&\quad - 2\big(uu_{xx} + u_x^2\big)(p+n) + u_x[(1-4u)n_x - (1+4u)p_x] - k^2(p+n)(1-u^2)\big\} - k_y^2\big), \\
\mathcal{L}_{1,1}^{(1)} &= \big\{2\lambda u\big[u_{xxx} - k_y^2 u_x\big] + 4\beta u u_x[12u^2 - 7 + \xi] - \zeta[4uu_x(p+n) + 2p_x(2u^2 - 1 + u) + 2n_x(2u^2 - 1 - u)]\big\} \\
\mathcal{L}_{1,1}^{(2)} &= \big\{1 + \beta[6u^4 - 7u^2 + 1 - \xi(1-u^2)] + \zeta(p+n)(1-u^2) + 2\lambda k_y^2(1-u^2)\big\},
\end{aligned}$$

$$\mathcal{L}_{1,3} = \zeta[(1+u)(1-u^2)]\partial_x^2 - 2\zeta u_x\left[2u^2+u-1\right]\partial_x - \zeta\left\{2uu_x^2 - u_{xx}(1-u^2) + k_y^2(1+u)(1-u^2)\right\},$$
$$\mathcal{L}_{1,4} = \zeta[(u-1)(1-u^2)]\partial_x^2 - 2\zeta u_x[2u^2-u-1]\partial_x - \zeta\left\{2uu_x^2 - u_{xx}(1-u^2) + k_y^2(u-1)(1-u^2)\right\},$$
$$\mathcal{L}_{2,2} = \partial_x^2 + 1 - k_y^2 + (1-u^2)/\tau,$$
$$\mathcal{L}_{3,1} = D_p\zeta p(1+u)\partial_x^2 + D_p\zeta[p_x(1+u) + 2pu_x]\partial_x + \left\{D_p\zeta\left[pu_{xx} + p_xu_x - k_y^2p(1+u)\right] - 2\chi u/\tau\right\},$$
$$\mathcal{L}_{3,3} = D_p\partial_x^2 + D_p[\phi_x + \zeta u_x(1+u)]\partial_x + \left(D_p\left\{\phi_{xx} - k_y^2 + \zeta\left[u_{xx}(1+u) + u_x^2\right]\right\} - \gamma n\right),$$
$$\mathcal{L}_{3,5} = D_p\left\{p\hat{\partial}_x^2 + p_x\hat{\partial}_x - k_y^2p\right\},$$
$$\mathcal{L}_{4,1} = D_n\zeta n(u-1)\partial_x^2 + D_n\zeta[n_x(u-1) + 2nu_x]\partial_x + \left\{D_n\zeta\left[nu_{xx} + n_xu_x - k_y^2n(u-1)\right] - 2\chi u/\tau\right\},$$
$$\mathcal{L}_{4,4} = D_n\partial_x^2 + D_n[-\phi_x + \zeta u_x(u-1)]\partial_x + \left(D_n\left\{-\phi_{xx} - k_y^2 + \zeta\left[u_{xx}(u-1) + u_x^2\right]\right\} - \gamma p\right),$$
$$\mathcal{L}_{4,5} = -D_n\left\{n\hat{\partial}_x^2 + n_x\hat{\partial}_x - k_y^2n\right\},$$

note that for simplicity, we dropped the subscript ℓ for all variables while the subscripts x represent derivatives with respect to the argument.

For the numerical computations, we approximate the spatial operators ∂_x and ∂_x^2 with periodic boundary conditions by [51]

$$\mathcal{G} \approx \frac{1}{2\Delta x}\begin{pmatrix} 0 & 1 & & & & -1 \\ -1 & 0 & 1 & & & \\ & -1 & 0 & 1 & & \\ & & & \ddots & & \\ & & & -1 & 0 & 1 \\ 1 & & & & -1 & 0 \end{pmatrix}, \quad \mathcal{D} \approx \frac{1}{\Delta x^2}\begin{pmatrix} -2 & 1 & & & & 1 \\ 1 & -2 & 1 & & & \\ & 1 & -2 & 1 & & \\ & & & \ddots & & \\ & & & 1 & -2 & 1 \\ 1 & & & & 1 & -2 \end{pmatrix},$$

where empty entries are zeros and Δx is the spatial distance between two points on the uniform grid. Similarly, to effectively eliminate potential jumps, the operators $\hat{\partial}_x$ and $\hat{\partial}_x^2$ with homogeneous Dirichlet boundary conditions are approximated by

$$\hat{\mathcal{G}} \approx \frac{1}{2\Delta x}\begin{pmatrix} 0 & 1 & & & & \\ -1 & 0 & 1 & & & \\ & -1 & 0 & 1 & & \\ & & & \ddots & & \\ & & & -1 & 0 & 1 \\ & & & & -1 & 0 \end{pmatrix}, \quad \hat{\mathcal{D}} \approx \frac{1}{\Delta x^2}\begin{pmatrix} -2 & 1 & & & & \\ 1 & -2 & 1 & & & \\ & 1 & -2 & 1 & & \\ & & & \ddots & & \\ & & & 1 & -2 & 1 \\ & & & & 1 & -2 \end{pmatrix},$$

and similarly for higher order derivatives.

In Fig. 4, we show two numerical realizations that produce the instabilities schematically depicted in Fig. 1, for different MP well depths $\xi = 2.65$ [in Fig. 4(a)] and $\xi = 2.8$ [in Fig. 4(b)] while keeping illumination fixed, $G = 8$. The dispersion relations (η_{ZZ} and η_{CR}) indicate that while in both cases the ZZ (odd symmetry) mode is unstable for $G > G_{ZZ}$, the CR (even symmetry) mode becomes unstable [with $\eta_{CR}(k_y^{max}) > 0$] only above $G = G_{CR}$; in Figs. 4(c) and 4(d), we also show the corresponding $\tilde{u}$ component of the eigenfunctions for the ZZ or the CR modes at k_y^{max}.

We generalize the results in a parameter plane spanned by (G, ξ) (see Fig. 5) and show that a similar trend also persists (dashed lines) for the asymmetric donor-acceptor ratio. The instability *onsets* are defined such that the maximal growth rate becomes positive, i.e., when $\eta(k_y^{max}) > 0$, at G_{ZZ} and G_{CR}, respectively. This implies degeneracy above the CR mode, $G > G_{CR}$, in a region where a competition between bending and pinching of stripes should be expected (even though the ZZ mode has a larger growth rate, $\eta_{ZZ} > \eta_{CR}$). Next, we show that this degeneracy is removed once we allow passage of current through the boundaries in the y direction, i.e., physical boundary conditions.

B. Realization of instability modes in the presence of charge outflux

Although in the above analysis we used nonphysical boundary conditions, as we did not allow charge flux through the boundaries in the y direction, the results provide a good guide for realistic charge-flux boundary conditions [41]. We validate these results by performing direct numerical simulations using (6) with outflux of charges through the y boundaries, assuming that these represent the charge collectors (i.e., electrodes) [36]:

$$\left(J_y^u, J_y^\chi, J_y^p, J_y^n, \phi\right)^T\big|_{y=0} = \left(0, 0, -D_p p\frac{\partial\phi}{\partial y}, 0, \frac{V}{2}\right)^T,$$
$$\left(J_y^u, J_y^\chi, J_y^p, J_y^n, \phi\right)^T\big|_{y=l_y} = \left(0, 0, 0, -D_n n\frac{\partial\phi}{\partial y}, -\frac{V}{2}\right)^T,$$

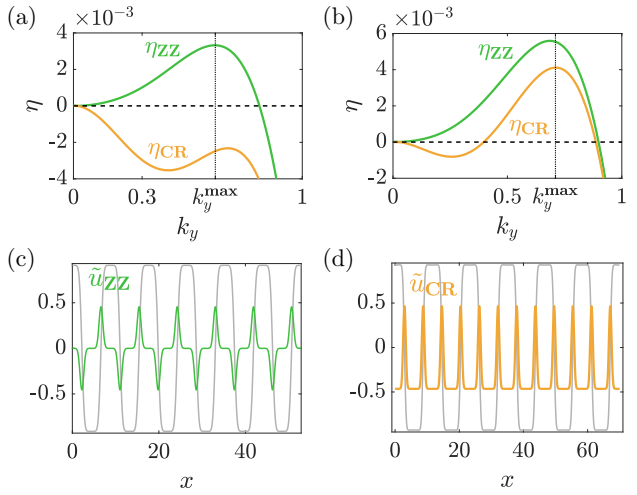

FIG. 4. (a) Dispersion relations, as computed from (6), showing the growth rates of the unstable ZZ (η_{ZZ}, green) and the stable CR (η_{CR}, orange) modes at $\xi = 2.65$ with $l_x = 6\ell_c$ and $\ell_c \approx 8.81$; at k_y^{max}, η_{ZZ} is maximal. (b) Same as (a), but for $\xi = 2.8$ with $l_x = 6\ell_c$ and $\ell_c \approx 11.66$, where also the CR mode is unstable; here, k_y^{max} marks the maximum of η_{CR}. (c) Normalized eigenfunctions of the ZZ instability, $\tilde{u}_{ZZ}(x)$, centered around $u = 0$ and rescaled to one-half the amplitude of the periodic solution, u_ℓ (gray line) for $\xi = 2.65$. (d) Same as (c), but for the CR eigenfunction $\tilde{u}_{CR}(x)$ (orange) at $\xi = 2.8$. Parameters: $G = 8$ and other parameters as in Fig. 3.

where $V = 0$ is a fixed voltage under short circuit conditions, and the fluxes (in their dimensionless forms) are

$$\mathbf{J}^u = D_u(1-u^2)\nabla\frac{\delta\mathcal{E}}{\delta u}, \quad \mathbf{J}^\chi = \chi\nabla\frac{\delta\mathcal{E}}{\delta\chi},$$

$$\mathbf{J}^p = D_p\, p\nabla\frac{\delta\mathcal{E}}{\delta p}, \quad \mathbf{J}^n = D_n\, n\nabla\frac{\delta\mathcal{E}}{\delta n}.$$

In the x direction, we employ periodic BC for all fields.

At low illumination values, $G < G_{ZZ}$, we find that the stripes are stable (left inset in Fig. 5). In the region $G_{ZZ} < G < G_{CR}$, the stripes are unstable only to ZZ, which as can be expected develops in the bulk (middle inset in Fig. 5). The agreement with the linear analysis is excellent and reproduces a similar wave number $k_y^{max} = 0.62$, as shown by the green curves in the middle inset.

In contrast, for $G > G_{CR}$, the primary instability now develops near the y boundaries and is of a cross-roll mode type (right inset in Fig. 5). Consequently, the charge-flux boundary conditions remove the degeneracy of the ZZ and the CR modes by enhancing the latter. The results are nevertheless, in agreement with the linear analysis (see orange lines near the boundaries) for both the developed wave numbers and the onsets [as shown by the dots (symmetric case) and inverted triangles (asymmetric case)]. Consequently, these results indicate that decreasing ξ and thus pronouncing the mixing energy towards a triple well, shifts the instability onsets to higher G values. The latter, in turn, suggests that the OPV will become less susceptible to deformation modes that enhance morphological degradation, in particular the dangerous CR instability.

V. DISCUSSION

Following recent highlights of a three-phase (donor-mixed-acceptor) bulk heterojunction (BHJ) in organic photovoltaics (OPV) [25,32,33,35], we used a mean-field approach [36] to identify the role of the intermediate mixed phase on morphological changes. Under illumination, the model is driven out of equilibrium so that stripe morphology may arise (Fig. 3). In contrast, under dark conditions, the system evolves solely by coarsening [35,41]. From a mathematical point of view, stripe morphology arises due to a finite wave-number instability [36] that is possible only under illumination and whose nature is affected by the order parameter and the exciton-electron-hole fields [see system (6)]. We focus on and distinguish between two generic transverse instabilities of donor-acceptor stripes in 2D (distinctly from the formation of stripes by phase separation) with symmetric and asymmetric compositions (as summarized in Fig. 5): the bending (zigzag mode) and the pinching (cross-roll mode). The pinching mode is characterized by high mixing energy, whereas at low mixing energies bending of the donor-acceptor domains is favored. We emphasize that the timescale separation between the morphological (material) changes and charge dynamics is of several orders of magnitude so that our results indicate only the initial trend and not necessarily convergence to a final state, but the further evolution, in reality, is extremely slow. Furthermore, the slow time evolution of the material lowers the sensitivity of the OPV to finite-amplitude perturbations, and thus the effect, for example, of sudden changes in illumination is negligible.

Although we limited our analysis to 2D, standard theory shows that the pinching mode may also lead to discontinuous and isolated domains in 3D [52–55], and thus, in OPV, loss of current to the electrodes that cause operation failure. This phenomenon resembles the so-called pearling of cylindrical threads [56–60]. Moreover, according to numerical simulations, relatively large D-A volumes of BHJ are more susceptible to transverse instabilities since the intermediate phase does not suppress transverse front instabilities that arise due to curvature effects as in bistable systems [61–64], i.e., in the direction that is parallel to the electrodes. This is consistent with the diffusion length of about tens of nanometer size of the BHJ [16,25].

Consequently, our analysis suggests that the qualitative significance of three-phase BHJ goes beyond inhibition of phase separation [35], as it may have *tailoring by demand* properties that can be controlled by the composition of the mixed phase via donor-acceptor choices: by decreasing the mixing energy parameter ξ, the instability onsets are shifted to higher illumination values G. This degree of control is absent or less sequential in two-phase OPV. We believe that our results may assist in the future design of long-lasting OPV, consisting of three-phase BHJ. In a broader context, our results should apply to other systems in physicochemical systems that exhibit phase separation [65,66] and can be driven

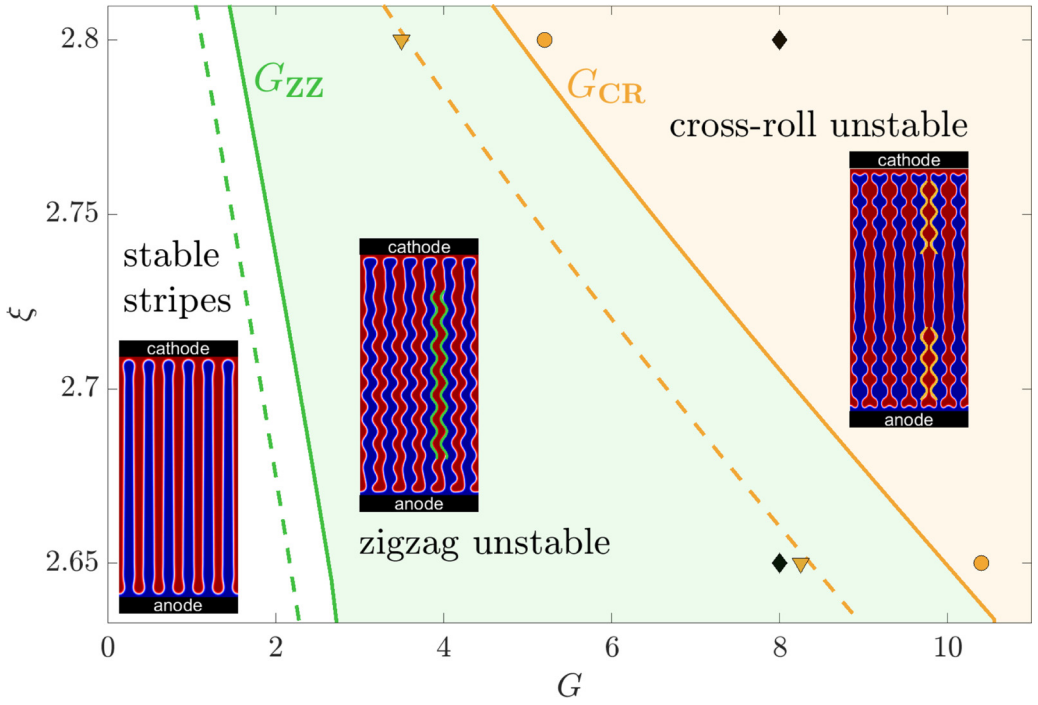

FIG. 5. Parameter plane (G, ξ), corresponding to illumination (G) and mixing energy (ξ), showing the instability regions of stripes. Solid (dashed) lines denote the onsets G_{ZZ} and G_{CR} for the symmetric $\langle u \rangle = 0$ (asymmetric $\langle u \rangle = 0.1$) D-A ratio, as obtained from (8), while • and ▼ correspond to onsets obtained by numerical integration of (6) with periodic boundary conditions in the x direction and charge flux in the y direction [36] (see text for details). The insets show snapshots of u obtained by direct numerical integration of (6): the left inset is the asymptotic solution at $(G, \xi) = (2, 2.65)$, the middle inset is for $(G, \xi) = (8, 2.65)$ and $t = 2800$ as indicated by the bottom diamond, and the right inset is for $(G, \xi) = (8, 2.8)$ and $t = 1200$ as indicated by the top diamond. The green and orange envelope lines in the middle and the right insets represent the ZZ and the CR modes, respectively, as obtained by eigenvalue analysis (8): the modes are parameterized as $x = (4 \mp 1/4)\ell_c - \varepsilon \cos(k_y^{\max} y)$ with $\varepsilon = 0.15$ and $k_y^{\max} = 0.62$, as indicated in Fig. 4(a), and $x = (4 \mp 1/4)\ell_c \pm \varepsilon \cos(k_y^{\max} y)$ with $\varepsilon = 0.15$ and $k_y^{\max} = 0.71$, as indicated in Fig. 4(b), respectively. The simulations were performed on a domain $\Omega = [0, 6\ell_c] \times [0, 100]$: for ZZ with $\ell_c \approx 8.81$ in x at $\xi = 2.65$ and for CR with $\ell_c \approx 11.66$ at $\xi = 2.8$. Other parameters are as in Fig. 3.

out of equilibrium, in particular in ion-intercalated renewable batteries that depend on reversible phase exchanges in charge and discharge cycling [67–69], such as in Li-based [70–72] and Ni-based [73–75] electrodes.

ACKNOWLEDGMENTS

The research was done in the framework of the Grand Technion Energy Program (GTEP) and of the Ben-Gurion University (BGU) Energy Initiative Program, and supported by the Adelis Foundation for renewable energy research.

[1] G. P. Kini, S. J. Jeon, and D. K. Moon, Adv. Mater. **32**, 1906175 (2020).
[2] H. S. Vogelbaum and G. Sauvé, Synth. Met. **223**, 107 (2017).
[3] A. Bonasera, G. Giuliano, G. Arrabito, and B. Pignataro, Molecules **25**, 2200 (2020).
[4] R. Zhou, Z. Jiang, C. Yang, J. Yu, J. Feng, M. A. Adil, D. Deng, W. Zou, J. Zhang, K. Lu, W. Ma, F. Gao, and Z. Wei, Nat. Commun. **10**, 5393 (2019).
[5] M. He, F. Qiu, and Z. Lin, J. Mater. Chem. **21**, 17039 (2011).
[6] J. U. Lee, J. W. Jung, J. W. Jo, and W. H. Jo, J. Mater. Chem. **22**, 24265 (2012).
[7] N. Grossiord, J. M. Kroon, R. Andriessen, and P. W. M. Blom, Org. Electron. **13**, 432 (2012).
[8] B. A. Collins, J. R. Tumbleston, and H. Ade, J. Phys. Chem. Lett. **2**, 3135 (2011).
[9] F. Liu, Y. Gu, J. W. Jung, W. H. Jo, and T. P. Russell, J. Polym. Sci., Part B: Polym. Phys. **50**, 1018 (2012).
[10] D. R. Kozub, K. Vakhshouri, L. M. Orme, C. Wang, A. Hexemer, and E. D. Gomez, Macromolecules **44**, 5722 (2011).
[11] K. Vakhshouri, D. R. Kozub, C. Wang, A. Salleo, and E. D. Gomez, Phys. Rev. Lett. **108**, 026601 (2012).
[12] C. J. Schaffer, C. M. Palumbiny, M. A. Niedermeier, C. Jendrzejewski, G. Santoro, S. V. Roth, and P. Müller-Buschbaum, Adv. Mater. **25**, 6760 (2013).
[13] C. J. Schaffer, C. M. Palumbiny, M. A. Niedermeier, C. Burger, G. Santoro, S. V. Roth, and P. Müller-Buschbaum, Adv. Energy Mater. **6**, 1600712 (2016).
[14] H. B. Naveed, K. Zhou, and W. Ma, Acc. Chem. Res. **52**, 2904 (2019).
[15] W. R. Mateker and M. D. McGehee, Adv. Mater. **29**, 1603940 (2017).

[16] M. Jørgensen, K. Norrman, S. A. Gevorgyan, T. Tromholt, B. Andreasen, and F. C. Krebs, Adv. Mater. **24**, 580 (2012).

[17] B. A. Collins, E. Gann, L. Guignard, X. He, C. R. McNeill, and H. Ade, J. Phys. Chem. Lett. **1**, 3160 (2010).

[18] J. Zhao, A. Swinnen, G. Van Assche, J. Manca, D. Vanderzande, and B. Van Mele, J. Phys. Chem. B **113**, 1587 (2009).

[19] N. D. Treat, M. A. Brady, G. Smith, M. F. Toney, E. J. Kramer, C. J. Hawker, and M. L. Chabinyc, Adv. Energy Mater. **1**, 82 (2011).

[20] S. Kouijzer, J. J. Michels, M. van den Berg, V. S. Gevaerts, M. Turbiez, M. M. Wienk, and R. A. Janssen, J. Am. Chem. Soc. **135**, 12057 (2013).

[21] N. D. Treat and M. L. Chabinyc, Annu. Rev. Phys. Chem. **65**, 59 (2014).

[22] I. Cardinaletti, J. Kesters, S. Bertho, B. Conings, F. Piersimoni, J. D'Haen, L. Lutsen, M. Nesladek, B. Van Mele, G. Van Assche, K. Vandewal, A. Salleo, D. Vanderzande, W. Maes, and J. V. Manca, J. Photon. Energy **4**, 040997 (2014).

[23] U. Vongsaysy, D. M. Bassani, L. Servant, B. Pavageau, G. Wantz, and H. Aziz, J. Photon. Energy **4**, 040998 (2014).

[24] K. Zhou, J. Liu, M. Li, X. Yu, R. Xing, and Y. Han, J. Phys. Chem. C **119**, 1729 (2015).

[25] W. Ma, J. R. Tumbleston, L. Ye, C. Wang, J. Hou, and H. Ade, Adv. Mater. **26**, 4234 (2014).

[26] O. Reid, J. Malik, G. Latini, S. Dayal, N. Kopidakis, C. Silva, N. Stingelin, and G. Rumbles, J. Polym. Sci., Part B: Polym. Phys. **50**, 27 (2012).

[27] J. Razzell-Hollis, W. C. Tsoi, and J.-S. Kim, J. Mater. Chem. C **1**, 6235 (2013).

[28] J. Bartelt, Z. Beiley, E. Hoke, W. Mateker, J. Douglas, B. Collins, J. Tumbleston, K. Graham, A. Amassian, H. Ade, J. Fréchet, M. Toney, and M. Mcgehee, Adv. Energy Mater. **3**, 364 (2013).

[29] T. Burke and M. McGehee, Adv. Mater. **26**, 1923 (2014).

[30] P. Müller-Buschbaum, Adv. Mater. **26**, 7692 (2014).

[31] N. Gasparini, X. Jiao, T. Heumueller, D. Baran, G. J. Matt, S. Fladischer, E. Spiecker, H. Ade, C. J. Brabec, and T. Ameri, Nat. Energy **1**, 16118 (2016).

[32] K. Zhou, J. Xin, and W. Ma, ACS Energy Lett. **4**, 447 (2019).

[33] C. Wang, X. Xu, W. Zhang, S. B. Dkhil, X. Meng, X. Liu, O. Margeat, A. Yartsev, W. Ma, J. Ackermann *et al.*, Nano Energy **37**, 24 (2017).

[34] F. Liu, W. Zhao, J. R. Tumbleston, C. Wang, Y. Gu, D. Wang, A. L. Briseno, H. Ade, and T. P. Russell, Adv. Energy Mater. **4**, 1301377 (2014).

[35] S. B. Dkhil, M. Pfannmöller, M. I. Saba, M. Gaceur, H. Heidari, C. Videlot-Ackermann, O. Margeat, A. Guerrero, J. Bisquert, G. Garcia-Belmonte *et al.*, Adv. Energy Mater. **7**, 1601486 (2017).

[36] A. Z. Shapira, N. Gavish, and A. Yochelis, Europhys. Lett. **125**, 38001 (2019).

[37] W. Ma, J. R. Tumbleston, M. Wang, E. Gann, F. Huang, and H. Ade, Adv. Energy Mater. **3**, 864 (2013).

[38] N. Gavish, I. Versano, and A. Yochelis, SIAM J. Appl. Dyn. Syst. **16**, 1946 (2017).

[39] A. Z. Shapira, H. Uecker, and A. Yochelis, Chaos: Interdiscip. J. Nonlinear Sci. **30**, 073104 (2020).

[40] M. C. Cross and P. C. Hohenberg, Rev. Mod. Phys. **65**, 851 (1993).

[41] G. A. Buxton and N. Clarke, Phys. Rev. B **74**, 085207 (2006).

[42] H. Uecker and D. Wetzel, SIAM J. Appl. Dyn. Syst. **13**, 94 (2014).

[43] T. Dohnal, J. D. Rademacher, H. Uecker, and D. Wetzel, in *Proceedings of 8th European Nonlinear Dynamics Conference, ENOC 2014*, edited by H. Ecker, A. Steindl, and S. Jakubek (Institute of Mechanics and Mechatronics, Vienna University of Technology, 2014).

[44] H. S. Greenside and W. M. Coughran Jr., Phys. Rev. A **30**, 398 (1984).

[45] H. S. Greenside and M. C. Cross, Phys. Rev. A **31**, 2492 (1985).

[46] U. Thiele and E. Knobloch, Phys. Fluids **15**, 892 (2003).

[47] T. Kolokolnikov, M. J. Ward, and J. Wei, Stud. Appl. Math. **116**, 35 (2006).

[48] T. Kolokolnikov, W. Sun, M. Ward, and J. Wei, SIAM J. Appl. Dyn. Syst. **5**, 313 (2006).

[49] J. Burke and E. Knobloch, Chaos **17**, 037102 (2007).

[50] J. A. Diez, A. G. González, and L. Kondic, Phys. Fluids **24**, 032104 (2012).

[51] W. H. Press, S. A. Teukolsky, W. T. Vetterling, and B. P. Flannery, *Numerical Recipes: The Art of Scientific Computing*, 3rd ed. (Cambridge University Press, Cambridge, 2007).

[52] X. Yu and J. T. Liu, Phys. Fluids **6**, 736 (1994).

[53] V. V. Kolmychkov, O. S. Mazhorova, Y. P. Popov, P. Bontoux, and M. El Ganaoui, C. R. Mech. **333**, 739 (2005).

[54] E. Fedoseev, V. Kolmychkov, and O. Mazhorova, Intl. J. Prog. Comput. Fluid Dyn. **10**, 208 (2010).

[55] H. Uecker and D. Wetzel, Physica D **406**, 132383 (2020).

[56] I. Tsafrir, D. Sagi, T. Arzi, M.-A. Guedeau-Boudeville, V. Frette, D. Kandel, and J. Stavans, Phys. Rev. Lett. **86**, 1138 (2001).

[57] P. Nelson, T. Powers, and U. Seifert, Phys. Rev. Lett. **74**, 3384 (1995).

[58] K. P. Sinha, S. Gadkari, and R. M. Thaokar, Soft Matter **9**, 7274 (2013).

[59] S. Chaïeb and S. Rica, Phys. Rev. E **58**, 7733 (1998).

[60] T. T. Nguyen, A. Gopal, K. Y. C. Lee, and T. A. Witten, Phys. Rev. E **72**, 051930 (2005).

[61] R. E. Goldstein, D. J. Muraki, and D. M. Petrich, Phys. Rev. E **53**, 3933 (1996).

[62] A. Yochelis, C. Elphick, A. Hagberg, and E. Meron, Physica D **199**, 201 (2004).

[63] A. Hagberg, A. Yochelis, H. Yizhaq, C. Elphick, L. Pismen, and E. Meron, Physica D **217**, 186 (2006).

[64] T. Kolokolnikov and M. Tlidi, Phys. Rev. Lett. **98**, 188303 (2007).

[65] H. Emmerich, Adv. Phys. **57**, 1 (2008).

[66] S. DeWitt and K. Thornton, in *Computational Materials System Design*, edited by D. Shin and J. Saal (Springer, Cham, 2018), pp. 67–87.

[67] J. L. Kaufman, J. Vinckevičiūtė, S. Krishna Kolli, J. Gabriel Goiri, and A. Van der Ven, Philos. Trans. R. Soc. A **377**, 20190020 (2019).

[68] A. Renuka Balakrishna, Y.-M. Chiang, and W. C. Carter, Phys. Rev. Materials **3**, 065404 (2019).

[69] A. Van der Ven, Z. Deng, S. Banerjee, and S. P. Ong, Chem. Rev. **120**, 6977 (2020).

[70] M. Tang, W. C. Carter, and Y.-M. Chiang, Annu. Rev. Mater. Res. **40**, 501 (2010).
[71] D. Grazioli, M. Magri, and A. Salvadori, Comput. Mech. **58**, 889 (2016).
[72] Y. Zhao, P. Stein, Y. Bai, M. Al-Siraj, Y. Yang, and B.-X. Xu, J. Power Sourc. **413**, 259 (2019).
[73] G. Briggs and M. Fleischmann, Trans. Faraday Soc. **67**, 2397 (1971).
[74] R. Barnard, C. Randell, and F. Tye, J. Appl. Electrochem. **10**, 109 (1980).
[75] R. Huggins, H. Prinz, M. Wohlfahrt-Mehrens, L. Jörissen, and W. Witschel, Solid State Ion. **70**, 417 (1994).